

# Ultrafast optical control of entanglement between two quantum-dot spins

Danny Kim, Samuel G. Carter, Alex Greilich, Allan S. Bracker and Daniel Gammon\*

**The interaction between two quantum bits enables the creation of entanglement, the two-particle correlations that are at the heart of quantum information science. In semiconductor quantum dots, much work has focused on demonstrating control over single spin qubits using optical techniques. However, optical control of two spin qubits remains a major challenge for scaling to a fully fledged quantum-information platform. Here, we combine advances in vertically stacked quantum dots with ultrafast laser techniques to achieve optical control of the entangled state of two electron spins. Each electron is in a separate InAs quantum dot, and the spins interact through tunnelling, where the tunnelling rate determines how rapidly entangling operations can be carried out. We achieve two-qubit gates with an interaction rate of 30 GHz, more than an order of magnitude faster than demonstrated in any other system so far. These results demonstrate the viability and advantages of optically controlled quantum-dot spins for multi-qubit systems.**

Semiconductor quantum dots (QDs) were among the first candidates proposed for solid-state qubits<sup>1</sup>. Self-assembled InAs QDs are a particularly versatile platform, because they are epitaxially grown in a semiconductor wafer and can be fabricated into a monolithic architecture containing both electronic<sup>2</sup> and photonic<sup>3</sup> circuit elements. Individual QDs themselves can be organized into more complex ‘molecules’ in one, two and three dimensions<sup>4</sup>. With these engineering advantages, one can anticipate an entire quantum network<sup>5</sup> with the scalability and stability of a solid-state system<sup>6</sup>.

The elementary optical excitation of a QD, the exciton, has a resonance frequency in the optical regime, giving QDs a great speed advantage over nuclear spins (radiofrequency) or electron spins (microwaves). With the giant optical dipole of a semiconductor QD, quantum operations can be carried out at a terahertz rate or faster<sup>7</sup>. Coherent manipulations of exciton qubits were some of the earliest quantum gate demonstrations in the solid state<sup>8–11</sup>.

Unfortunately, the exciton lifetime is less than a nanosecond in a QD, so in practice they are inadequate as qubits. This problem is solved by charging the QD with a single electron, and using the long-lived electron spin as the qubit. The electron spin lives for milliseconds<sup>12</sup> or longer and has a coherence time of microseconds<sup>13–16</sup>. The exciton now acts as an auxiliary state for ultrafast conversion between optical coherence and spin coherence<sup>17</sup>.

The opportunity created by this optically controlled spin paradigm has produced a burst of recent activity in single-qubit operations with QDs, including single-spin initialization<sup>18–20</sup>, non-destructive readout<sup>20,21</sup> and fast spin manipulation<sup>22–26</sup>. However, the power of quantum information originates from entanglement of multiple qubits, and so far all of these efforts are limited to a single isolated qubit. Creating and controlling entanglement requires a well-controlled spin interaction between QDs, and quantum optical techniques that can address individual QDs within a pair. The interaction needs to be strong enough to maintain the speed advantage of optically controlled QDs, but not so strong that individual control of dots is impractical.

Here, we go beyond one QD qubit, demonstrating the fabrication and optical control of a two-qubit system consisting of two electron spins, each on separate tunnel-coupled QDs.

We establish concurrently the three important prerequisites for two-qubit entanglement control: (1) initialization of the two-electron spin state through optical pumping; (2) single-qubit gates using short laser pulses; (3) and two-qubit gates using longer laser pulses. To achieve single-qubit gates in a multiple-qubit system, the key is to use a pulse so short that the two dots do not have time to interact while a single spin is optically rotated. For two-qubit gates we use pulses that are longer than the interaction time between the dots. Combining all of these techniques, we obtain optical control of two QD qubits on a timescale that is much faster than any other candidate for quantum computing<sup>27–29</sup>.

## Tunnel-coupled QDs

Controlled entanglement of two spins requires an interaction between the spins, the strength of which determines how fast the two-qubit gate can be carried out. A number of entanglement mechanisms have been proposed for optically driven QD spins, including coupling through photons and optical cavity modes<sup>17,30,31</sup>, and through Coulomb and/or tunnelling interactions between neighbouring dots<sup>32–36</sup>. Here we employ the kinetic exchange interaction based on coherent tunnelling. Tunnelling provides the largest interaction rate, and because of recent advances in the growth and spectroscopy of vertically stacked QDs (refs 37–40) can be precisely controlled through a combination of quantum size engineering and applied electric field bias. This interaction has also been used in electrically defined QDs<sup>27,41</sup>, although the interaction is much stronger in our self-assembled QD system—30 GHz as compared with ~2 GHz (ref. 27), allowing an order of magnitude faster gate speeds.

For this study, two vertically stacked self-assembled InAs QDs were grown with a thin tunnel barrier of GaAs/AlGaAs such that the electrons can coherently tunnel between the dots (Fig. 1). We grew the two QDs with different thicknesses so that they have different optical transition energies. As a result each is optically addressable with a resonant laser frequency. The QDs are incorporated into a Schottky diode so that by adjusting the voltage bias each QD is charged with a single electron.

The calculated Hund–Mulliken model of the  $2e$  energy level system<sup>42</sup> is shown in Fig. 2. Using optical transmission

<b>Report Documentation Page</b>			Form Approved OMB No. 0704-0188		
<p>Public reporting burden for the collection of information is estimated to average 1 hour per response, including the time for reviewing instructions, searching existing data sources, gathering and maintaining the data needed, and completing and reviewing the collection of information. Send comments regarding this burden estimate or any other aspect of this collection of information, including suggestions for reducing this burden, to Washington Headquarters Services, Directorate for Information Operations and Reports, 1215 Jefferson Davis Highway, Suite 1204, Arlington VA 22202-4302. Respondents should be aware that notwithstanding any other provision of law, no person shall be subject to a penalty for failing to comply with a collection of information if it does not display a currently valid OMB control number.</p>					
1. REPORT DATE <b>MAR 2011</b>	2. REPORT TYPE	3. DATES COVERED <b>00-00-2011 to 00-00-2011</b>			
4. TITLE AND SUBTITLE <b>Ultrafast optical control of entanglement between two quantum-dot spins</b>			5a. CONTRACT NUMBER	5b. GRANT NUMBER	
			5c. PROGRAM ELEMENT NUMBER		
6. AUTHOR(S)			5d. PROJECT NUMBER	5e. TASK NUMBER	
			5f. WORK UNIT NUMBER		
7. PERFORMING ORGANIZATION NAME(S) AND ADDRESS(ES) <b>Naval Research Laboratory, Washington, DC, 20375</b>			8. PERFORMING ORGANIZATION REPORT NUMBER		
9. SPONSORING/MONITORING AGENCY NAME(S) AND ADDRESS(ES)			10. SPONSOR/MONITOR'S ACRONYM(S)		
			11. SPONSOR/MONITOR'S REPORT NUMBER(S)		
12. DISTRIBUTION/AVAILABILITY STATEMENT <b>Approved for public release; distribution unlimited</b>					
13. SUPPLEMENTARY NOTES					
14. ABSTRACT					
15. SUBJECT TERMS					
16. SECURITY CLASSIFICATION OF:			17. LIMITATION OF ABSTRACT <b>Same as Report (SAR)</b>	18. NUMBER OF PAGES <b>7</b>	19a. NAME OF RESPONSIBLE PERSON
a. REPORT <b>unclassified</b>	b. ABSTRACT <b>unclassified</b>	c. THIS PAGE <b>unclassified</b>			

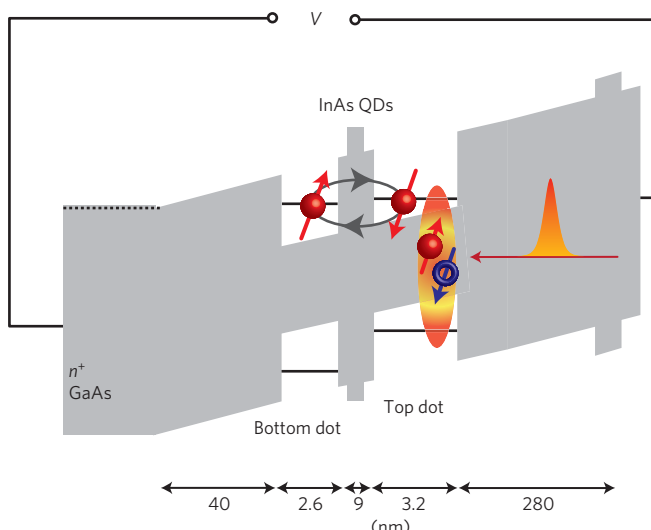


**Figure 1 | Sample structure.** Schematic of the Schottky diode structure by which two electrons are charged into separate QDs. The spins in the two QDs are coupled by coherent tunnelling through a 9 nm GaAs/Al<sub>0.3</sub>Ga<sub>0.7</sub>As/GaAs (3/3) barrier. Laser fields are used to initialize, measure or rotate the spins through a real or virtual electron–hole pair (exciton) resonantly excited in the top dot.

spectroscopy, the 2e charge state was found to be stable for a bias range of 100 mV centred at about 0.46 V. Beyond this range 1 and 3 electrons are more stable in the QD pair. Within this 2e stability range the lowest energy configuration consists of one electron residing in each dot. As a result of the Pauli exclusion principle, the two electrons can tunnel between QDs only if they have an antisymmetric spin state. The spin states are split into degenerate triplets ( $T_0 = |\uparrow\downarrow\rangle + |\downarrow\uparrow\rangle$ ,  $T_- = |\downarrow\downarrow\rangle$ ,  $T_+ = |\uparrow\uparrow\rangle$ ) and a lower-energy singlet ( $S = |\uparrow\downarrow\rangle - |\downarrow\uparrow\rangle$ ) with a kinetic exchange splitting  $\Delta_{ee}$  that is a result of tunnelling between the dots<sup>43</sup>. The magnitude of the exchange energy determines the interaction strength between dots and ultimately how fast the entanglement can be controlled. We found that an exchange energy of 30 GHz enables both ultrafast one- and two-qubit gates, as we will show.

The spin state is optically controlled through an exciton state ( $X^{2-}$ ), in which an electron–hole pair is created in the top dot. An exciton in the smaller bottom dot is tens of millielectronvolts higher in energy. Tunnelling between the two dots is rendered negligible in the optically excited state at the same bias (0.46 V) owing to additional Coulomb interaction energies<sup>42,44</sup>. We start at zero magnetic field, in which case the exciton state is fourfold degenerate, with the states labelled by their total spin projection  $m_z$  in Fig. 2. The optical selection rules at zero field (blue lines) show that both S and  $T_0$  couple to the same optically excited state, forming a  $\Lambda$ -level diagram, as required for optical spin control.

### Two-qubit initialization: Optical spin pumping

Optical spin initialization of the two-electron (2e) system is demonstrated by optical pumping. The two spectral lines in Fig. 3a arise from excitation of the 2e singlet and triplet states to the common exciton. The splitting between the lines gives a direct measure of the kinetic exchange energy ( $\Delta_{ee} \sim 125 \mu\text{eV} = 30 \text{ GHz}$ ). Figure 3a shows bleaching of the singlet and triplet absorption lines in the bias range between 0.45 and 0.48 V, that is the centre of the 2e charge stability plateau. This is a well-known signature of optical spin pumping in a  $\Lambda$ -level diagram<sup>18–20</sup>, where the spin is excited out of one spin state and becomes shelved in the other after a few recombination cycles. The pumping is efficient (at least 95% fidelity) as long as the optical cycle is faster than relaxation

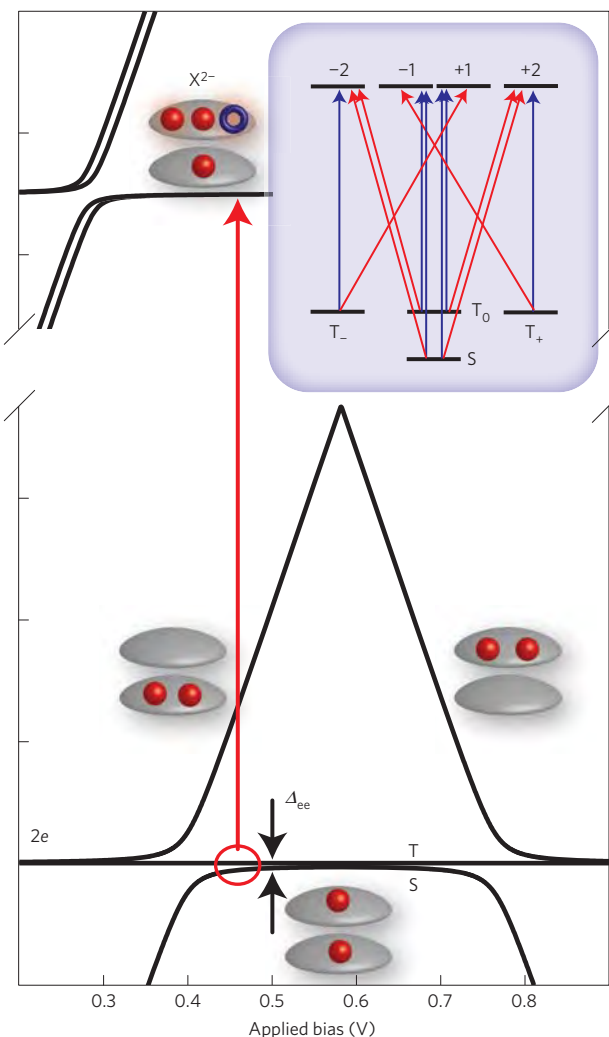


**Figure 2 | Energy levels of the 2e system.** Hund–Mulliken model of the 2e system showing the energy levels of the ground and lowest optically excited states, and their respective tunnelling anticrossings. The red arrow shows approximately the bias in which these experiments were conducted. Inset: Corresponding energy level diagram for spin substates (not to scale). The  $X^{2-}$  excited trion states are labelled by their total spin projection  $m_z$ . The selection rules at zero magnetic field are shown by blue arrows (circularly polarized). In a transverse magnetic field additional transitions, shown by red arrows, become fully allowed, and the blue and red transitions are linearly polarized and orthogonal.

between the S and T ground states. Near the edges of the stability plateau (white dashed lines in Fig. 3a), spin-flip cotunnelling to the doping layer results in efficient ground-state relaxation, and no net pumping is possible. The spin pumping can be defeated by repumping on the opposite branch of the  $\Lambda$ -system using a second laser as shown in the two linescans in Fig. 3c.

The selection rules of Fig. 2 (inset) indicate that two of the triplet sublevels ( $T_+$  and  $T_-$ ) are not part of a  $\Lambda$ -diagram and therefore should not pump at zero magnetic field. However, as shown by the experiment, the triplet absorption signal is almost completely suppressed through optical pumping. This implies that there is weak mixing of the triplets through the hyperfine interaction and/or heavy-hole/light-hole mixing in the exciton states. These interactions turn on additional weak optical transitions and allow full initialization into the singlet state.

Although spin initialization through optical pumping may seem routine, in this case incoherent pumping is in fact generating a

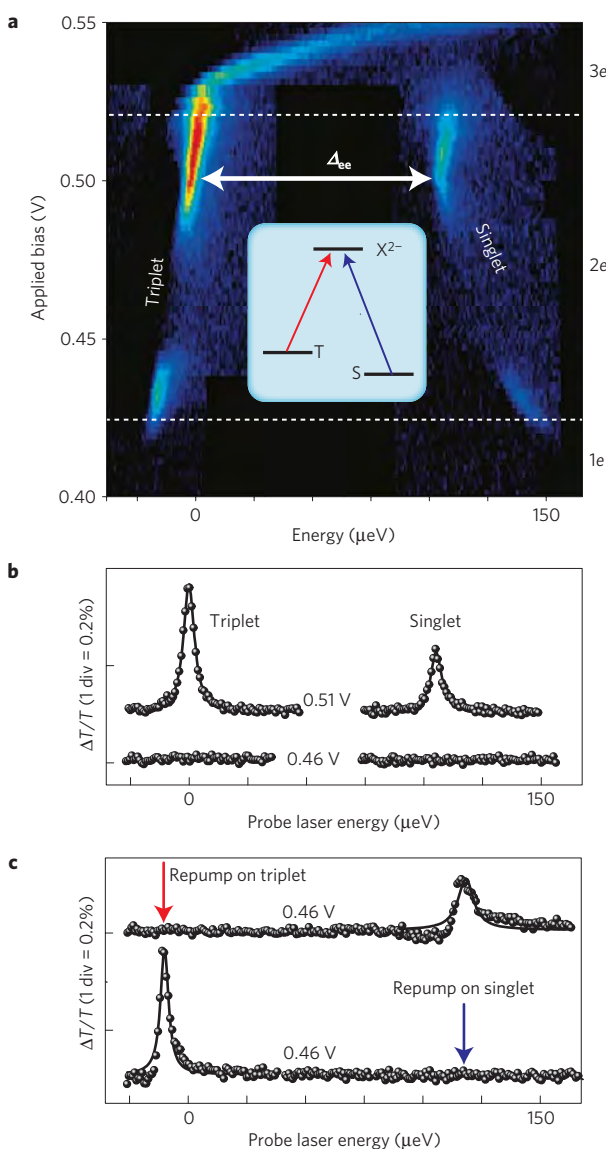


**Figure 3 | Optical spin pumping of the two-electron state.** **a**, Intensity plot of the single-laser transmission spectrum as a function of bias. The zero in the energy scale is at 1.3 eV. The dashed horizontal lines indicate the edges of the two-electron stability plateau. Inset:  $\Lambda$ -diagram with the singlet and triplet coupling to the same  $X^{2-}$  state. **b**, Single-laser linescan spectra at two bias values: one in the cotunnelling regime that shows triplet and singlet peaks (0.51 V) and one in the pumping regime where the peaks are gone (0.46 V). **c**, These traces show that the transmission signals at 0.46 V are restored by tuning the frequency of a second repumping laser to the opposite arm of the  $\Lambda$ -system.

particular entangled spin state,  $S = |\uparrow\downarrow\rangle - |\downarrow\uparrow\rangle$ . This entanglement is possible owing to the exchange interaction. It may seem strange at first to consider the individual spin states as qubits and the singlet an entangled state because the exchange interaction is always coupling the two spins. Nevertheless, we can independently manipulate the individual spin states using optical pulses that act faster than this interaction. This allows us to transform the singlet state into a variety of other entangled states.

#### Entanglement control using pairs of single-qubit gates

For single-qubit gates we use short, circularly polarized pulses (13 ps) with a bandwidth (146  $\mu$ eV) larger than the exchange splitting but much less than the splitting between excitons in the

top and bottom dots (Fig. 4a). As the pulses are shorter than the exchange interaction time and because the exciton is localized in the top dot, the pulse acts only on the spin in this dot. The pump laser pulses are detuned below the triplet transition by  $\sim 270 \mu$ eV, allowing a single-spin rotation with only virtual occupation of the  $X^{2-}$  exciton state<sup>22,24,26</sup>. This single-qubit gate induces a relative phase between the up and down spin states in just the top dot—a rotation of this spin about the optical axis. As shown previously for a single electron spin, a circularly polarized  $\pi$ -rotation takes  $|\downarrow\rangle - |\uparrow\rangle$  into  $|\downarrow\rangle - e^{i\pi}|\uparrow\rangle = |\downarrow\rangle + |\uparrow\rangle$ , (refs 22,24–26,45). Similarly, in this two-electron case, where the pulse acts only on the top dot, the  $\pi$ -pulse rotates  $S = |\uparrow\downarrow\rangle - |\downarrow\uparrow\rangle$  into  $T_0 = |\uparrow\downarrow\rangle + |\downarrow\uparrow\rangle$ .

By applying two such single-spin rotations separated by a delay time during which the  $2e$  spin state precesses, we can control the  $2e$  state. Initialization into the singlet state again is achieved with the continuous-wave (cw) probe laser tuned to the triplet transition, which also acts as the measurement. At zero magnetic field, we operate in the  $S$  and  $T_0$  subspace, which can be visualized as a Bloch sphere as shown in Fig. 4b. The first pulse rotates the  $2e$  state from  $S$  to a superposition with  $T_0$ , with a rotation angle that depends on the laser power. For example, an effective  $\pi/2$ -pulse rotates the Bloch vector to the equator as shown in Fig. 4b. Between pulses, the state precesses around the Bloch sphere at the frequency of the exchange splitting ( $\Delta_{ee}$ ). The second pulse drives the state either up or down depending on the phase of the superposition state. The projection onto  $T_0$  determines the population and the corresponding signal of the cw probe.

Figure 4c (upper curves) shows the oscillations in the signal as a function of pulse delay, called Ramsey fringes. The frequency of these oscillations (30 GHz) corresponds to the exchange energy  $\Delta_{ee}$ , which is a function of bias voltage. The observed frequencies as a function of bias (red dots in Fig. 4d) are in excellent agreement with the measured singlet–triplet splitting (red dashed curve in Fig. 4d). The oscillations have a decay time of 400–700 ps, depending on bias, although this can be substantially increased. The main damping source is found to be fluctuations in electric field that produce fluctuations in the exchange energy. This is seen in Fig. 4d, where the bias dependence of the decay has been fitted to the derivative of the exchange energy ( $\delta\Delta_{ee}/\delta V$ ) multiplied by the voltage fluctuation amplitude of 3.8 mV, taken as the fitting parameter. These fluctuations probably arise from background charges in the sample. This contribution can be removed by designing the molecule such that  $\delta\Delta_{ee}/\delta V = 0$  within the stability range of the  $2e$  configuration. This would be accomplished by shifting the stability region of the  $2e$  configuration in Fig. 2 towards the right to  $\sim 0.6$  V. Additional dephasing contributions due to the cw initialization/measurement laser that is persistently on can be eliminated by turning this laser off during the precession in between pulses<sup>16</sup>. Hyperfine-induced coupling to the  $T_+ / T_-$  states is expected to lead to dephasing on a longer timescale, although a number of recent results on single QDs indicate that even this effect can be substantially reduced<sup>13–15</sup>.

The amplitude of the oscillations as a function of pulse intensity is plotted in Fig. 4e. The maximum amplitude occurs for two  $\pi/2$ -pulses, but decreases to nearly zero for two  $\pi$ -pulses, which should drive the system back to the initial  $S$  state, regardless of pulse delay. These oscillations as a function of laser power correspond to spin-Rabi oscillations, in which the Bloch vector can be driven all the way around the Bloch sphere. The amplitude dependence on the pulse intensity is not linear as expected from the adiabatic approximation. Instead the dependence is sublinear ( $P^{0.7}$ ), which indicates that the detuning is insufficient for adiabatic elimination of the exciton state<sup>24</sup>. The combination of laser pulse area and delay time permits the controlled generation of any entangled superposition state within this part of the  $2e$  spin phase space, that is  $\alpha|\uparrow\downarrow\rangle + \beta|\downarrow\uparrow\rangle$ .

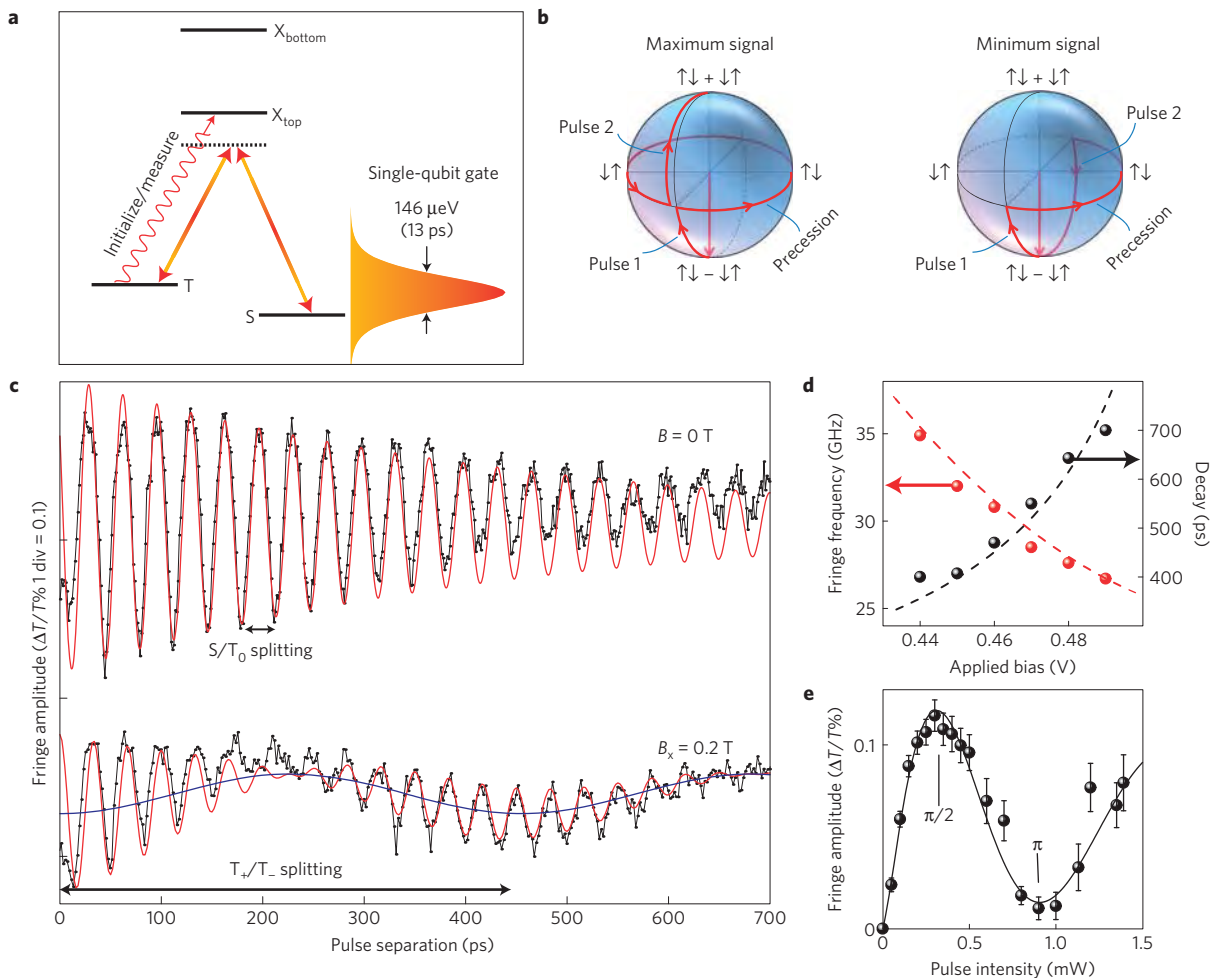


**Figure 4 | Coherent control of the 2e spin state using two 13 ps pulses with a variable time delay.** **a**, Single-qubit gate schematic where a short pulse is used, with a bandwidth greater than the singlet-triplet splitting. **b**, Bloch sphere representation of spin control within the  $S-T_0$  subspace. The spin state is initialized to the south pole ( $S = |\uparrow\downarrow\rangle - |\downarrow\uparrow\rangle$ ). The first pulse coherently drives the Rabi vector up, after which it precesses around the sphere. The second pulse drives the vector either up or down depending on the time separation between pulses and thereby leads to oscillations in the measurement. **c**, Upper curve: the resulting Ramsey interference oscillations in the  $T_0$  transmission signal as a function of the pulse separation time, with zero magnetic field. Lower curve: Ramsey interference obtained at 0.2 T showing two frequency components, comprising the faster  $S-T_0$  splitting (30 GHz) and the slower  $T_+/T_-$  splitting (2.2 GHz). The latter frequency is at twice the single-electron Zeeman splitting ( $g_e = -0.4$ ). **d**, Measured Ramsey fringe frequency and decay time as a function of bias voltage at 0 T. The dashed line for the fringe frequency is the measured singlet-triplet splitting ( $\Delta_{ee}$ ) from Fig. 3a. The dashed line for the decay time is a calculation of the expected dephasing time due to voltage fluctuations of  $\Delta_{ee}$  as discussed in the text. **e**, Fringe amplitude versus pulse intensity showing Rabi oscillations of the spin state. The solid line is a fit giving a single-qubit rotation fidelity of 98%. The error bars are obtained from the fits to the Ramsey fringes at each power and represent one standard error.

Optical control of the full 2e spin state is possible using a transverse magnetic field that allows Raman transitions to the  $T_+$  and  $T_-$  states<sup>46</sup> (see Fig. 2, inset). Figure 4c (lower curves) shows Ramsey fringes in a small transverse magnetic field of 0.2 T, which now show frequency components associated with  $T_+$  and  $T_-$ . In a transverse magnetic field, the spin eigenstates are in a different basis with spins oriented along the magnetic field instead of the optical axis. In the optical basis, a short pulse rotates  $S \rightarrow T_0$ . It can be seen by rewriting  $S$  and  $T_0$  in the field basis that a short pulse now rotates  $S \rightarrow T_+ - T_-$ . The superposition of  $T_+$  and  $T_-$ ,  $|\uparrow\uparrow\rangle - |\downarrow\downarrow\rangle$ , precesses at twice the single-electron Zeeman frequency. Calculated Ramsey fringes in this magnetic field are shown in Fig. 4c and reproduce the experimental result very well. In this model, the populations of the  $T_0$  and  $T_\pm$  states after both pulses are  $(1/2)W^2[1 - \cos(\omega_+ - \omega_-)\Delta t]$  and  $W(1 - W)[1 + \cos\omega_\pm\Delta t]$ , respectively. The frequencies  $\omega_\pm$  represent the  $S-T_\pm$  splittings,  $W$  is related to the single pulse area  $\Theta$  through  $W = \sin^2(\Theta/2)$ , and  $\Delta t$  is the delay between pulses. We have observed that by using a

$\pi$ -pulse, full rotation to this  $T_+/T_-$  subspace is possible where then only these slower oscillations at  $\omega_+ - \omega_-$  are observed. These results show that we have extended the subspace from  $S-T_0$  to include the  $T_+$  and  $T_-$  states.

### Two-qubit phase gate

It may seem surprising in these Ramsey fringe experiments that we can control the entangled state using only single-qubit rotations. In reality the exchange interaction that causes precession on the Bloch sphere acts as a two-qubit gate, with the timing between pulses effectively controlling the interaction time. A direct way to control the 2e state is with longer, narrowband pulses that act as two-qubit phase gates. In analogy with pulse rotations developed for single QDs (refs 26,45), a narrowband pulse near-resonant with an energy eigenstate that drives the system up to an excited state and then back down (a  $2\pi$ -pulse) induces a phase change. For example, an optical  $2\pi$ -pulse driving the singlet state gives  $|\uparrow\downarrow\rangle - |\downarrow\uparrow\rangle \Rightarrow e^{i\phi}(|\uparrow\downarrow\rangle - |\downarrow\uparrow\rangle)$ , where  $\phi$  depends on

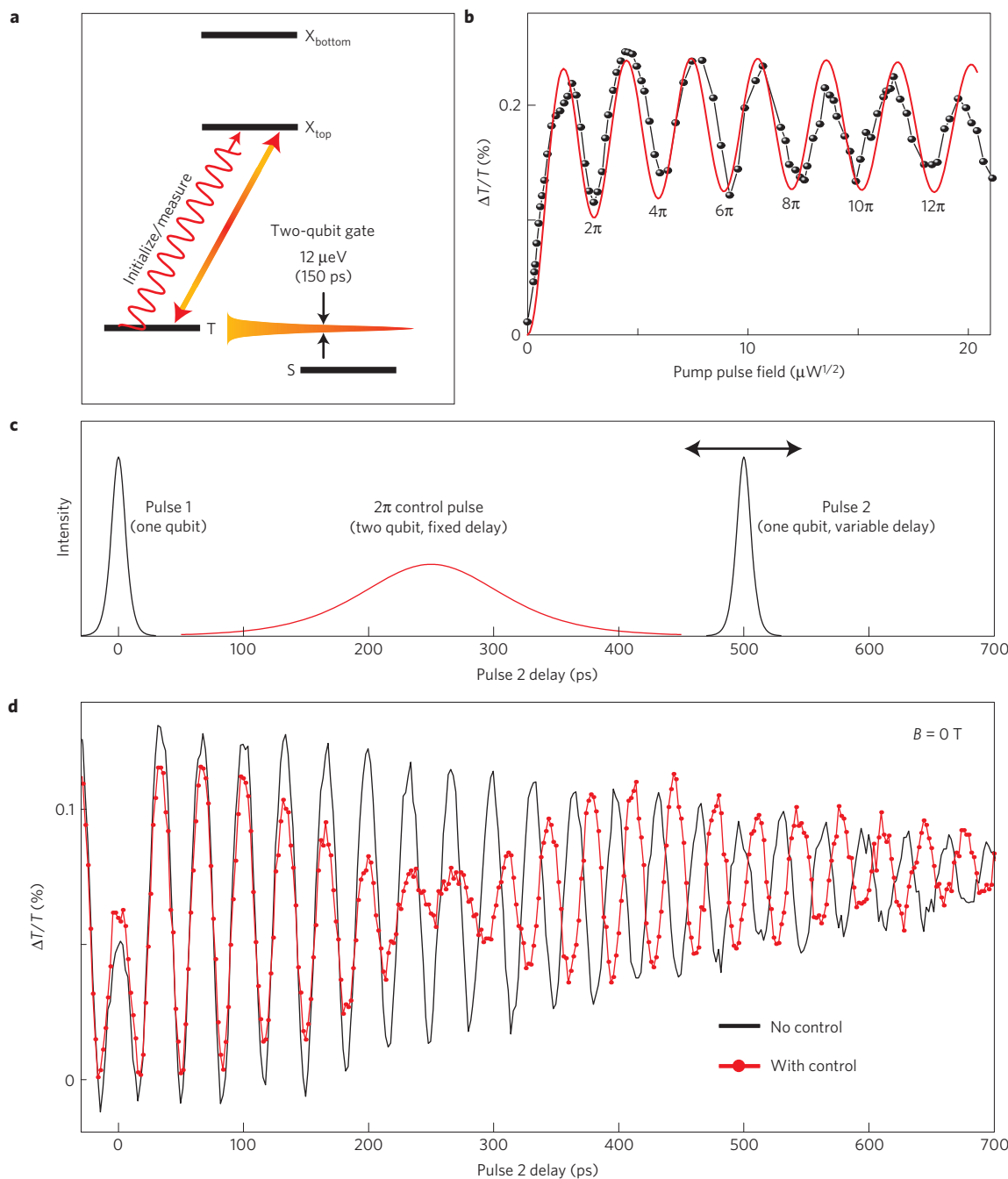


**Figure 5 | Two-qubit phase gate.** **a**, Two-qubit gate schematic in which a long pulse acts only on one of the ground states. **b**, With a pulsed pump laser ( $\sim 150$  ps pulse width) on the singlet, optical Rabi oscillations are observed with a period that scales with the square root of the pump intensity. **c**, Pulse sequence for a two-qubit phase gate experiment, where the second short pulse has variable time delay. **d**, Ramsey interference oscillations with and without a two-qubit control pulse near-resonant with the triplet. The fidelity of the two-qubit phase gate is about 80%.

pulse detuning<sup>25,26,45</sup>. When this gate with  $\phi = \pi/2$  (often called square-root-of-swap) acts on a product state,  $|\uparrow\downarrow\rangle$ , the result is an entangled state,  $|\uparrow\downarrow\rangle - i|\downarrow\uparrow\rangle$ .

To obtain this two-qubit phase gate, we first demonstrate optical Rabi oscillations (Fig. 5b). A pulsed laser with a relatively narrow bandwidth of  $12 \mu\text{eV}$  ( $\sim 150$  ps pulse width), much less than the singlet-triplet splitting, is used to coherently drive the singlet transition. The cw probe is tuned to the triplet transition. As the pulse intensity increases, the triplet transmission signal shows Rabi oscillations that are periodic with the field amplitude (square root of the average laser power). The absorption signal does not return to zero owing to recombination during these long pulses,

as reproduced by a simulation using optical Bloch equations in a three-level model (red curve in Fig. 5b).

The two-qubit phase gate is demonstrated by placing a  $2\pi$ -pulse, in this case near-resonant with the triplet transition, after the first short pulse of a Ramsey fringe experiment (see Fig. 5a,c). Pulse 1 rotates the Bloch vector up near the equator, where it precesses, and the longer control pulse changes the phase. Pulse 2 is used to measure these dynamics as a function of time by rotating the vector up or down, depending on its phase. In Fig. 5d, the oscillating signal goes nearly to zero during the control pulse, as the triplet population is excited to the exciton. As the exciton is driven back down to the triplet, the oscillations return with a phase change of

145°. We have been able to vary this phase between  $-180^\circ$  and  $180^\circ$  by changing the pulse detuning.

## Outlook

We have demonstrated ultrafast optical control of two electron spins in two separate QDs using optical initialization, single-qubit gates with short pulses, and two-qubit gates with longer pulses or through precession in the exchange field. Local entanglement between the two spins is inferred from the coherent evolution of superposition states as measured in Ramsey fringes. The fringes indicate that we have generated a nearly pure quantum state of two spins, which cannot be written as a product state. A direct measure of entanglement could be carried out by probing correlations in the individual spin states on a timescale faster than the interaction.

One might ask whether spin qubits based on the singlet and triplets or the individual spin states are most natural. These pictures are formally equivalent, and both are useful. Our main motivation for treating the qubit system as two individual spins is that we can manipulate the spins independently with ultrafast pulses. However, we find that the simplest explanation of the Ramsey fringes is provided in the S–T<sub>0</sub> basis using the Bloch sphere illustration of Fig. 4a, which naturally accounts for precession in the exchange field. This same duality is present in many systems, including NMR-based quantum computing in molecules<sup>47</sup> and quantum transport in electrically defined QDs (ref. 27,48). Moreover, in quantum transport studies, it has been pointed out that a S–T<sub>0</sub> qubit is of special interest because of its weaker sensitivity to nuclear fluctuations.

An important remaining question is what operations are sufficient and most convenient to obtain universal control, allowing us to span the entire phase space. A well-known route to universal control is single-qubit gates for each QD and an entangling two-qubit gate<sup>49</sup>. Taking this approach would require single-qubit gates about an arbitrary axis for both QDs. Extending short-pulse spin rotations to the bottom QD should be straightforward, and rotation about an arbitrary axis has been demonstrated in single QDs (ref. 24). A potential challenge in our system is to carry out single-qubit rotations about the magnetic field axis without a simultaneous two-qubit interaction. This is a consequence of having the exchange interaction in the ground state, which continually couples the qubits as they are also precessing about the magnetic field. Ultimately it may be useful to adapt techniques from NMR, such as refocusing pulses to effectively turn off the exchange interaction<sup>47</sup>. Decoupling the spins in the ground state could also be achieved through quantum state engineering. For example, we may engineer the coupling of the spin qubits to occur only in the exciton states<sup>20,40,43</sup> through variations in structural design. This would turn on the interaction only when required, and the ultrafast optical techniques demonstrated here would still be applicable.

We emphasize that one of the main advantages of this optically functional QD system is its natural coupling to photons, which can act as flying qubits for quantum communication. For example, the spin entanglement in the dots could be transferred to entanglement of emitted photons<sup>50</sup>. Perhaps most exciting is the potential for further scaling using a quantum network, an approach to quantum computing or communication in which a set of nodes are entangled through quantum channels<sup>5,30</sup>. These locally entangled spin qubits are ideal as a node in a distributed quantum network connected through photons<sup>6</sup>. For error suppression it is necessary to have within each node at least two qubits in which fast entanglement control is possible, as demonstrated here<sup>6</sup>.

## Methods

**Sample structure.** Two vertically stacked InAs dots were grown by molecular beam epitaxy on an n+-doped GaAs substrate (see Fig. 1). The QDs are embedded

in a GaAs Schottky diode, which allows for deterministic charging and for tuning of energy levels through the quantum-confined Stark effect. The sample consists of an n-type Si-doped buffer layer, a 40 nm GaAs spacer barrier and the two InAs dot layers separated by a 9 nm GaAs/AlGaAs/GaAs barrier. A 280 nm GaAs capping layer with a 25 nm AlGaAs current blocking layer was included 10 nm from the surface. The top dot was grown thicker such that it would have the lower optical transition, and such that electrons would tunnel but holes would not<sup>44</sup>. The nominal dot thicknesses are 2.6 and 3.2 nm for the bottom and top dot, respectively. To obtain an appropriate tunnelling rate we increased the height of the barrier by incorporating 3 nm of Al<sub>0.3</sub>Ga<sub>0.7</sub>As in between two 3 nm layers of GaAs; giving a total barrier thickness of only 9 nm. The actual anticrossing energy is  $2t_c = 700 \mu\text{eV}$  as measured from photoluminescence. With pure GaAs, a 20 nm barrier would be required to obtain the same tunnelling rate. The energy between the singlet and triplet (exchange energy) at the bias where the 2e configuration is stable was  $\sim 125 \mu\text{eV}$ . The sample's optical transition spectrum and charging behaviour as a function of bias were determined by photoluminescence as discussed in earlier studies<sup>44</sup>.

**Measurement method.** For single-molecule studies, 1  $\mu\text{m}$  apertures were patterned in a 120-nm-thick Al layer using electron-beam lithography. A 5 nm layer of Ti was deposited before the Al. The sample was placed in a He-flow cryostat at 5 K. Piezo positioners were used for positioning. A 0.68-numerical-aperture aspheric lens was used to focus the laser to a diameter of  $\sim 2 \mu\text{m}$  on the aperture, and also to collect the light for the photoluminescence measurements. Light transmitted through the aperture was focused onto an avalanche photodiode. The transitions were probed by means of Stark-shift modulation spectroscopy using narrow-linewidth lasers (nanoelectronvolt range) and lock-in techniques. The sample was modulated with a 100-mV-amplitude square-wave voltage at 10 kHz superimposed on the fixed d.c. voltage. A 300 ms time constant was used for all of the experiments.

The single cw laser experiments were carried out with linearly polarized light. For the Rabi oscillation and Ramsey fringe experiments, one or two titanium:sapphire lasers were used, with circular polarizations opposite to that of the cw probe. The pump laser(s) for all of the multi-laser experiments were rejected using a polarization analyser. For the Ramsey fringe experiments, short pulses (13 ps) were detuned below the triplet transition by 270  $\mu\text{eV}$ , and long pulses ( $\sim 150 \mu\text{s}$ ), if present, were tuned resonant with the triplet.

**Simulations.** The Rabi oscillations shown in Fig. 5b were simulated with a three-level  $\lambda$ -system, in which S and T<sub>0</sub> couple to the same trion state (one of the  $m_z = \pm 1$  states) with equal dipole moments. The three-level density matrix equations are solved numerically in response to a 120 ps Gaussian pulse resonant with S. A recombination time of 500 ps is used (equally to both S and T<sub>0</sub>), and recombination during the pulse prevents the population from being driven fully back down to S.

Simulations of the Ramsey fringe experiment were also carried out, with 12 ps pulses detuned 300  $\mu\text{eV}$  from the centre of the transitions. These pulses rotated the Bloch vector from S towards T<sub>0</sub>, with little trion population remaining after the pulse. When the delay between pulses was varied, the T<sub>0</sub> population due to the pulses oscillated as observed experimentally. However, the pulses were not short enough to completely rotate the Bloch vector all the way to the T<sub>0</sub> state. We estimate that the series of two pulses used in these experiments were able to give a maximum of 65% population in the T<sub>0</sub> state. We have demonstrated a full rotation to the T<sub>0</sub> state by using shorter 3 ps pulses.

**Fidelity estimates.** The initialization fidelity of 95% is estimated from the bleaching of the triplet line in the single-laser differential transmission scans in Fig. 3b. At 0.46 V, where pumping occurs, any residual absorption is clearly within the noise, so we use the noise level as an upper bound on the residual signal. We compare this noise level with the triplet signal at 0.51 V, where pumping is inhibited by rapid cotunneling. The fidelity is then  $F_{\text{pump}} = 1 - \alpha/\alpha_0 = 0.95$ , where  $\alpha$  is the noise level at 0.46 V and  $\alpha_0$  is the signal level at 0.51 V.

We estimate the fidelity of single-qubit gates using data from Fig. 4e, which plots the Ramsey fringe amplitude as a function of pulse power. The oscillations show decay that we attribute to pulse-induced decoherence. From the fit to a decaying cosine, we determine the expected amplitude for two  $\pi/2$ -pulses with no dephasing,  $A_{\text{fit}}$ , and compare this with the maximum signal at 0.3 mW,  $A_{\text{meas}}$ . If each pulse reduces the Bloch vector by a factor D, then  $D^2 = A_{\text{meas}}/A_{\text{fit}} = 0.935$ , giving a gate fidelity of  $F = (1+D)/2 = 0.98 \pm 0.01$  (ref. 24). Nominally, this is the gate fidelity for a  $\pi/2$ -pulse, but these 13 ps pulses are not short enough to rotate the Bloch vector all the way to the equator. From simulations, pulses that should give a  $\pi$ -pulse for a negligible exchange splitting only rotate the Bloch vector by a polar angle  $\sim\pi/3$ . This effect is not included in the fidelity calculation as it does not degrade the coherence of the state.

The fidelity of the two-qubit narrowband pulse is estimated from the ratio of the Ramsey fringe amplitude before the pulse (33 ps) and after (443 ps). This gives  $D = 0.61$  ( $F = 0.80$ ), which, surprisingly, is better than that expected from dephasing during this time period,  $\exp(-410/500) = 0.44$ . We speculate that the pulse is partially reversing the inhomogeneous dephasing from voltage fluctuations, but this effect is not yet understood.

Received 15 July 2010; accepted 25 October 2010; published online 19 December 2010

## References

- Lloyd, S. A potentially realizable quantum computer. *Science* **261**, 1569–1571 (1993).
- Warburton, R. J. *et al.* Optical emission from a charge-tunable quantum ring. *Nature* **405**, 926–929 (2000).
- Englund, D., Faraon, A., Zhang, B., Yamamoto, Y. & Vuckovic, J. Generation and transfer of single photons on a photonic chip. *Opt. Express* **15**, 5550–5558 (2007).
- Kiravittaya, S., Rastelli, A. & Schmidt, O. G. Advanced quantum dot configurations. *Rep. Prog. Phys.* **72**, 046502 (2009).
- Cirac, J. I., Zoller, P., Kimble, H. J. & Mabuchi, H. Quantum state transfer and entanglement distribution among distant nodes in a quantum network. *Phys. Rev. Lett.* **78**, 3221–3224 (1997).
- Benjamin, S. C., Lovett, B. J. & Smith, J. M. Prospects for measurement-based quantum computing with solid state spins. *Laser Photon. Rev.* **3**, 556–574 (2009).
- Chen, P., Piermarocchi, C. & Sham, L. J. Control of exciton dynamics in nanodots for quantum operations. *Phys. Rev. Lett.* **87**, 067401 (2001).
- Bonadeo, N. H. *et al.* Coherent optical control of the quantum state of a single quantum dot. *Science* **282**, 1473–1476 (1998).
- Stievater, T. H. *et al.* Rabi oscillations of excitons in single quantum dots. *Phys. Rev. Lett.* **87**, 133603 (2001).
- Zrenner, A. *et al.* Coherent properties of a two-level system based on a quantum-dot photodiode. *Nature* **418**, 612–614 (2002).
- Li, X. *et al.* An all-optical quantum gate in a semiconductor quantum dot. *Science* **301**, 809–811 (2003).
- Kroutvar, M. *et al.* Optically programmable electron spin memory using semiconductor quantum dots. *Nature* **432**, 81–84 (2004).
- Greibich, A. *et al.* Nuclei-induced frequency focusing of electron spin coherence. *Science* **317**, 1896–1899 (2007).
- Xu, X. *et al.* Optically controlled locking of the nuclear field via coherent dark-state spectroscopy. *Nature* **459**, 1105–1109 (2009).
- Brunner, D. *et al.* A coherent single-hole spin in a semiconductor. *Science* **325**, 70–72 (2009).
- Press, D. *et al.* Ultrafast optical spin echo in a single quantum dot. *Nature Photon.* **4**, 367–370 (2010).
- Imamoglu, A. *et al.* Quantum information processing using quantum dot spins and cavity QED. *Phys. Rev. Lett.* **83**, 4204–4207 (1999).
- Atature, M. *et al.* Quantum-dot spin-state preparation with near-unity fidelity. *Science* **312**, 551–553 (2006).
- Xu, X. *et al.* Fast spin state initialization in a singly charged InAs–GaAs quantum dot by optical cooling. *Phys. Rev. Lett.* **99**, 097401 (2007).
- Kim, D. *et al.* Optical spin initialization and nondestructive measurement in a quantum dot molecule. *Phys. Rev. Lett.* **101**, 236804 (2008).
- Atature, M., Dreiser, J., Badolato, A. & Imamoglu, A. Observation of Faraday rotation from a single confined spin. *Nature Phys.* **3**, 101–105 (2007).
- Berezovsky, J., Mikkelsen, M. H., Stoltz, N. G., Coldren, L. A. & Awschalom, D. D. Picosecond coherent optical manipulation of a single electron spin in a quantum dot. *Science* **320**, 349–352 (2008).
- Ramsay, A. J. *et al.* Fast optical preparation, control, and readout of a single quantum dot spin. *Phys. Rev. Lett.* **100**, 197401 (2008).
- Press, D., Ladd, T. D., Zhang, B. & Yamamoto, Y. Complete quantum control of a single quantum dot spin using ultrafast optical pulses. *Nature* **456**, 218–221 (2008).
- Greibich, A. *et al.* Ultrafast optical rotations of electron spins in quantum dots. *Nature Phys.* **5**, 262–266 (2009).
- Kim, E. D. *et al.* Fast spin rotations by optically controlled geometric phases in a charge-tunable InAs quantum dot. *Phys. Rev. Lett.* **104**, 167401 (2010).
- Petta, J. R. *et al.* Coherent manipulation of coupled electron spins in semiconductor quantum dots. *Science* **309**, 2180–2184 (2005).
- DiCarlo, L. *et al.* Demonstration of two-qubit algorithms with a superconducting quantum processor. *Nature* **460**, 240–244 (2009).
- Neumann, P. *et al.* Quantum register based on coupled electron spins in a room-temperature solid. *Nature Phys.* **6**, 249–253 (2010).
- Yao, W., Liu, R.-B. & Sham, L. J. Theory of control of the spin-photon interface for quantum networks. *Phys. Rev. Lett.* **95**, 030504 (2005).
- Clark, S. M., Fu, K.-M. C., Ladd, T. D. & Yamamoto, Y. Quantum computers based on electron spins controlled by ultrafast off-resonant single optical pulses. *Phys. Rev. Lett.* **99**, 040501 (2007).
- Piermarocchi, C., Chen, P., Sham, L. J. & Steel, D. G. Optical RKKY interaction between charged semiconductor quantum dots. *Phys. Rev. Lett.* **89**, 167402 (2002).
- Calarco, T., Datta, A., Fedichev, P., Pazy, E. & Zoller, P. Spin-based all-optical quantum computation with quantum dots: Understanding and suppressing decoherence. *Phys. Rev. A* **68**, 012310 (2003).
- Lovett, B. W. *et al.* Quantum computing with spin qubits interacting through delocalized excitons: Overcoming hole mixing. *Phys. Rev. B* **72**, 115324 (2005).
- Emary, C. & Sham, L. J. Optically controlled logic gates for two spin qubits in vertically coupled quantum dots. *Phys. Rev. B* **75**, 125317 (2007).
- Economou, S. E. & Reinecke, T. L. Optically induced spin gates in coupled quantum dots using the electron–hole exchange interaction. *Phys. Rev. B* **78**, 115306 (2008).
- Bracker, A. S. *et al.* Engineering electron and hole tunneling with asymmetric InAs quantum dot molecules. *Appl. Phys. Lett.* **89**, 233110 (2006).
- Stinaff, E. A. *et al.* Optical signatures of coupled quantum dots. *Science* **311**, 636–639 (2006).
- Krenner, H. J. *et al.* Optically probing spin and charge interactions in a tunable artificial molecule. *Phys. Rev. Lett.* **97**, 076403 (2006).
- Robledo, L. *et al.* Conditional dynamics of interacting quantum dots. *Science* **320**, 772–775 (2008).
- Foletti, S., Bluhm, H., Mahalu, D., Umansky, V. & Yacoby, A. Universal quantum control of two-electron spin quantum bits using dynamic nuclear polarization. *Nature Phys.* **5**, 903–908 (2009).
- Doty, M. F. *et al.* Optical spectra of doubly charged quantum dot molecules in electric and magnetic fields. *Phys. Rev. B* **78**, 115316 (2008).
- Scheibner, M. *et al.* Spin fine structure of optically excited quantum dot molecules. *Phys. Rev. B* **75**, 245318 (2007).
- Economou, S. E. & Reinecke, T. L. Theory of fast optical spin rotation in a quantum dot based on geometric phases and trapped states. *Phys. Rev. Lett.* **99**, 217401 (2007).
- Tureci, H. E., Taylor, J. M. & Imamoglu, A. Coherent optical manipulation of triplet–singlet states in coupled quantum dots. *Phys. Rev. B* **75**, 235313 (2007).
- Vandersypen, L. M. K. & Chuang, I. L. NMR techniques for quantum control and computation. *Rev. Mod. Phys.* **76**, 1037–1069 (2004).
- Koppens, F. H. L. *et al.* Driven coherent oscillations of a single electron spin in a quantum dot. *Nature* **442**, 766–771 (2006).
- Neilsen, M. A. & Chuang, I. L. *Quantum Computation and Quantum Information* (Cambridge Univ. Press, 2000).
- Economou, S. E., Lindner, N. & Rudolph, T. Optically generated 2-dimensional photonic cluster state from coupled quantum dots. *Phys. Rev. Lett.* **105**, 093601 (2010).

## Acknowledgements

This work was supported by NSA/ARO, ARO MURI, DARPA and ONR.

## Author contributions

All authors were involved in writing the manuscript. D.K. was involved in all aspects. S.G.C. was involved with conceiving and carrying out the experiments, and analysing and modelling the data. A.G. was involved with sample development and characterization. A.S.B. was involved with sample fabrication, development and characterization. D.G. was involved with conceiving the experiment, sample development and data analysis.

## Additional information

The authors declare no competing financial interests. Reprints and permissions information is available online at <http://npg.nature.com/reprintsandpermissions>. Correspondence and requests for materials should be addressed to D.G.